Analysis of Localized Plastic Strain in Heterogeneous Cast Iron Microstructures Using 3D Finite Element Simulations

Kent Salomonsson and Jakob Olofsson

Abstract The design and production of light structures in cast iron with high static and fatigue performance is of major interest in e.g. the automotive area. Since the casting process inevitably leads to heterogeneous solidification conditions and variations in microstructural features and material properties, the effects on multiple scale levels needs to be considered in the determination of the local fatigue performance. In the current work, microstructural features of different cast irons are captured by use of micro X-ray tomography, and 3D finite element models generated. The details of the 3D microstructure differ from the commonly used 2D representations in that the actual geometry is captured and that there is not a need to compensate for 3D-effects. The first objective with the present study is to try and highlight certain aspects at the micro scale that might be the underlying cause of fatigue crack initiation, and ultimately crack propagation, under fatigue loading for cast iron alloys. The second objective is to incorporate the gained knowledge about the microstructural behavior into multi-scale simulations at a structural length scale, including the local damage level obtained in the heterogeneous structure subjected to fatigue load.

Keywords Cast iron · Microstructure · X-ray tomography · Characterization

Introduction

The ever-increasing demands for lower emissions in the automotive industry require lighter components to be manufactured. Materials such as polymeric materials, aluminum and magnesium alloys have increased in use. However, there is a strong connection with lowered density and lowered strength. Thus, attention has also been turned towards the use of optimizing stronger materials topologically

K. Salomonsson (✉) · J. Olofsson
Jönköping University, School of Engineering, Materials and Manufacturing,
P.O. Box 1026, SE-551 10 Jönköping, Sweden
e-mail: kent.salomonsson@ju.se

to reduce weight. In this context, cast iron has been, and still is, beneficial to use when constructing components for the automotive industry since its manufacturability has several strong benefits such as e.g. high machinability, high heat resistance, good wear resistance. Different cast iron alloys have different benefits. For example, ductile iron or spherical graphite iron (SGI) has high strength and low thermal conductivity, whereas grey iron or lamellar graphite iron (LGI) has high thermal conductivity and lower strength. Compacted graphite (CGI) is thus of interest for components where e.g. both strength and thermal conductivity is sought after, e.g. engine blocks.

Determination of the mechanical properties for different cast iron alloys has gained interest over the past decade and specifically locally varying mechanical properties that result from e.g. the geometrical features of the component, chemical composition, cooling rates etc. [1]. Locally varying mechanical properties is traditionally not taken into account when performing strength analyses for e.g. automotive components [2]. It was shown by [3] that there are considerable differences when analyzing a component using isotropic homogenous properties compared to the use of locally varying material properties. The difference can be as high as 90 MPa locally [3]. The microstructures for SGI, LGI and CGI contain complex combinations of different phases such as e.g. graphite morphology, fractions of ferrite and/or pearlite which govern the mechanical performance of the material [1]. Thus, depending on the geometry of the component these parameters will change and as a result, the mechanical performance will change locally [3].

In the field of shape analysis, it is common practice to specify one global measure of the graphite particle and one concerning the morphology to determine different microstructural features [4]. Several parameters have been defined over the years that serve the purpose of defining particular properties specifically for compacted and lamellar graphite inclusions [5]. Several methods have been developed that propose to characterize microstructures, see e.g. [6–8]. The proposed methods use two-dimensional images in the characterization framework. The images provide a nodule count which is converted to the three-dimensional nodule count by determination of the area fraction of graphite and an assumption of average graphite diameter to yield the volume count. The assumption is that all the graphite nodules are of equal size and perfectly spherical for e.g. SGI. In the work by [9], they refined the expression and used a parametrized model to account for different sized and shaped nodules. The characterization of different cast iron alloys is frequently determined by the value of nodularity where values range between 65 and 90% for SGI and lower values correspond to CGI (10–25% nodularity) and LGI (0–5% nodularity), respectively.

Nevertheless, it has been shown that it is not the grade % of graphite that determines the shift in ultimate tensile strength (UTS) observed for different SGI alloys, but the grade % of pearlite and ferrite [10]. Interestingly, [10] showed that an increase in nodularity increases the UTS for SGI, whereas an increase of vermicularity decreases the UTS for CGI. It has been observed in e.g. [11] for SGI that underlying cause of this effect is due to the shape of graphite inclusions. In

particular, high local strains are observed experimentally in [11] by use of digital image correlation.

In the present paper, we analyze SGI, LGI and CGI microstructures by use of three-dimensional finite element models to try and highlight particular shapes and distances that localize plastic strain well below homogenized levels of strain at the structural scale. The three-dimensional numerical models modeled as representative volume elements with virtually the same size, i.e. $0.7 \times 0.7 \times 0.7$ mm. The paper is organized as follows. Firstly, we elaborate on the generation of the three-dimensional finite element models. Secondly, we characterize the microstructures by use of characterization parameters for two-dimensional approaches. The numerical models are presented next and the paper is finalized by the results and concluding remarks.

Generation of Microstructures

By use of micro X-ray tomography, it is possible to produce two-dimensional slices of a specimen. The size of the specimen is generally determined by the sought-after resolution one is aiming for. In the present work, the aim was to distinguish different phase morphologies. Pictures of different microstructures are depicted in Fig. 1.

In order to distinguish between different phases in the microstructure it is suggested that an image analysis is performed prior to segmentation of the images. Figure 2 illustrates an example for a SGI microstructure where the original micrograph is seen together with its corresponding probability density which is generated by use of the Fiji/ImageJ plugin Weka segmentation. The extent of the ferrite phase surrounding the graphite is clearly visible by observing Fig. 2.

The resolution in which one can determine the extent of different phases is related to the bit-depth as well. For the case of 8-bit pictures, the image intensity limited to values between 0 and 255, whereas for the 16-bit depth images between 0 and 4095. Thus, details in intensity shift can be captured more easily for the 16-bit images.
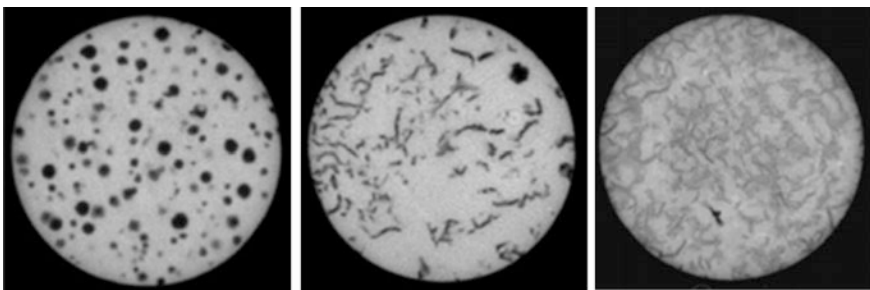

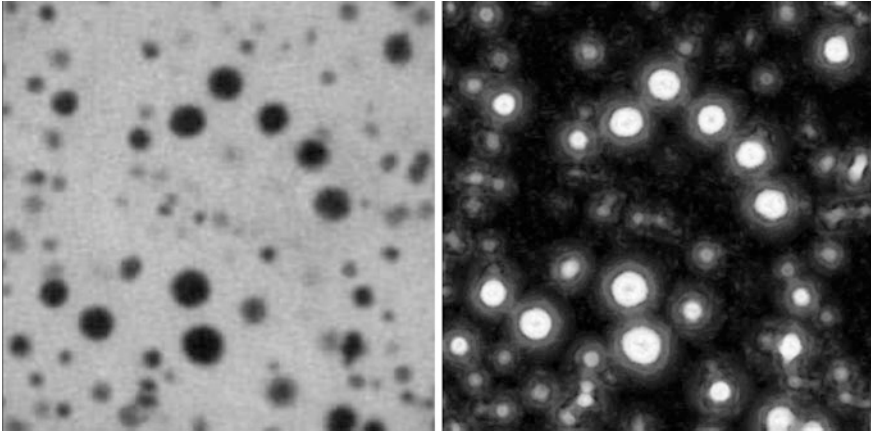**Fig. 1** Pictures taken from the X-ray tomograph. *Left* SGI, *center* CGI and *right* LGI

Fig. 2 Example of a SGI microstructure (*left*), probability density of intensity (*right*)

Once the images have been pre-analyzed using image analysis software, each image is segmented to establish the extent of each microstructural phase. The segmented images are then interpolated to yield a three-dimensional representation of the microstructure, see Fig. 3 and e.g. [12] for a fairly recent study on three-dimensional analysis using micro µCT to analyze SGI.

Fig. 3 Three-dimensional representation of the interpolated segmented images
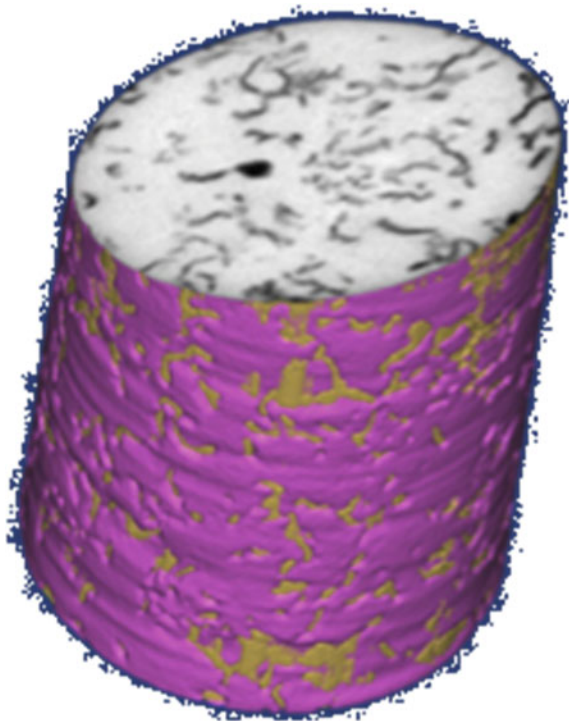
Numerical Model

The size of the representative volumes that were selected for SGI and LGI in the present study are about $0.7 \times 0.7 \times 0.7$ mm^3, whereas a cylinder is used for the CGI, see Fig. 4.

The numerical models contain different number of finite elements due phase morphology. Specifically, for the SGI microstructure it was essential to resolve the ferrite phase boundary surrounding the graphite inclusions. Thus, the number of elements used for SGI is approximately 5 million linear tetrahedral elements. The cylinder representing the CGI microstructure contains approximately 2.5 million linear tetrahedral elements and the final microstructure, LGI, contains approximately 4 million linear tetrahedral elements. For simplicity, the interfaces connecting different phases share nodes.

It should be noted that the carbide inclusions were considered virtually rigid in comparison to the surrounding phase pearlite and we, thus, chose to model carbide as elastic and homogenous with an artificially stiff Young's modulus of 300 GPa. The graphite was considered to be elastic and homogenous and since the Young's modulus for graphite varies significantly in literature, we chose to use 25 GPa. The ferrite and pearlite phases were modeled as elasto-plastic materials using a rate in-dependent Johnson-Cook material model. The material properties for the different phases and the different microstructures are presented in Table 1.

In order to analyze and load the microstructures, a displacement field is extracted from a structural analysis of an engine block mount for simplicity and to yield
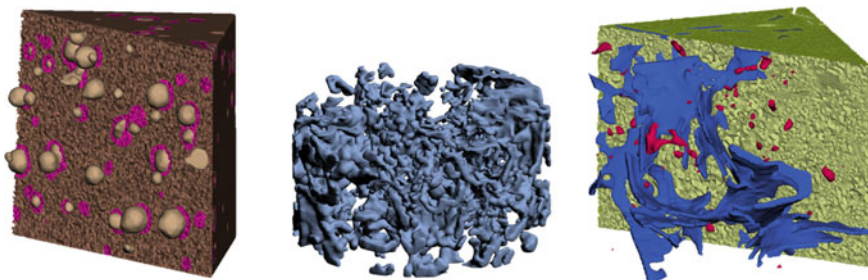

Fig. 4 Three-dimensional representations of SGI (*left*), CGI (*center*) and LGI (*right*)

Table 1 Material parameters used in the simulations. Young's modulus and Johnson-Cook parameters

	E [GPa]	A [MPa]	B [MPa]	n [−]
Graphite	25			
Ferrite [13]	197	175	571	0.35
Pearlite [13]	206	750	593	0.33
Carbide	300			

"actual" loading. The selected volume, from which the displacement field is extracted, can be seen in Fig. 5. This is also a region which was strained the most in the structural simulation.

The loading of the microstructures was in form of a controlled displacement vector, $u \approx (5.2, -3.5, 6.9)$ µm, of the top surface (positive z-direction according to Fig. 6) and the bottom surface is clamped. It should be noted that all the microstructures were loaded by the same displacement vector on the top surface (Fig. 6).
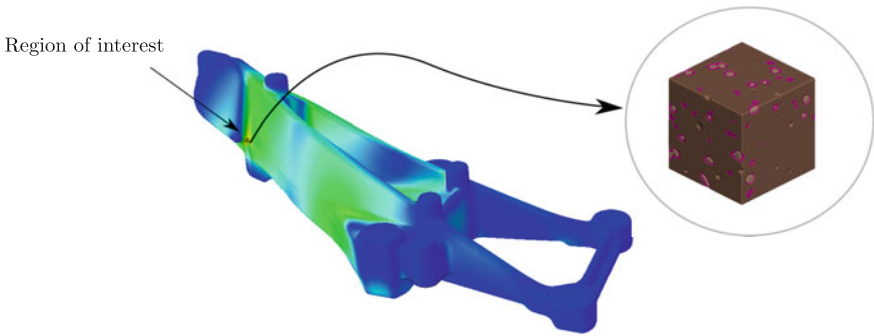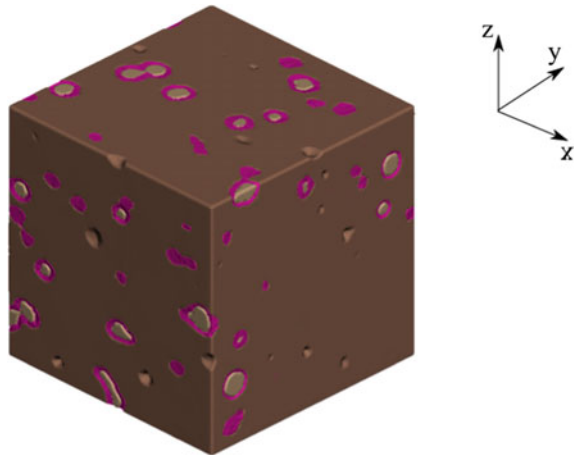

Fig. 5 Strained engine block mount with the selected region of interest

Fig. 6 Example of the SGI 3D microstructure with local coordinate system

Results

The intention of the present study is to highlight differences between different microstructures and compare the effective localized plastic strain development. Figure 7 shows the effective plastic strain for the three microstructures as a result of the controlled displacement vector. Clearly, the strains for the CGI microstructure are not directly comparable due to a the difference in the shape of the representative volume. Nevertheless, the SGI and the LGI microstructures are comparable and it can be observed that the SGI microstructure displays localized plastic strains which are not seen for the LGI microstructure. The ferrite phase surrounding the graphite nodules have a lower yield stress than the pearlite and the graphite inclusions act similar to voids. Thus, stress concentrations are expected around all graphite nodules that are loaded, which leads to the increased plastic strain primarily in the ferrite phase. For the LGI microstructure, the graphite inclusions are in form of large connected flakes which instead act as dampers that reduce the stress concentration. This effect can also be observed for the CGI with its vermicular graphite inclusions. Spherical inclusions are also present in CGI which will result in similar stress states as those observed for SGI.

Considering ultimate tensile stress levels, SGI will generally have the highest value followed by CGI and then LGI [14]. This is directly related to the localization of stress concentrators such as graphite inclusions and their shapes, respectively, see e.g. [15, 16]. Notice also that three-dimensional effects such as e.g. graphite nodules, will increase the strain locally, point A for SGI in Fig. 7, which is not possible to predict in a two-dimensional analysis of the corresponding microstructure, see Fig. 8.
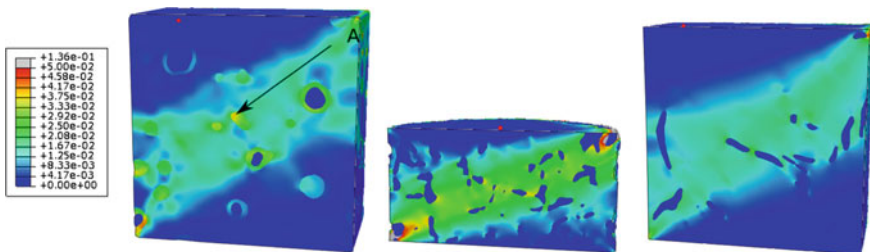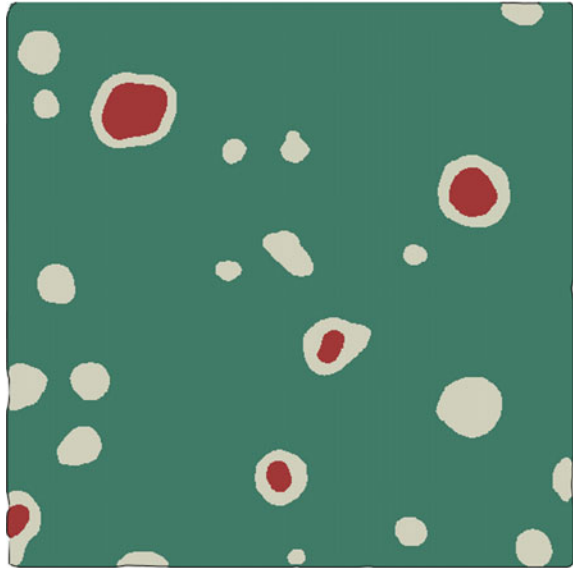

Fig. 7 Contour plots of a center cross section showing the equivalent plastic strain for the loaded microstructures; from *left* to *right*, SGI, CGI and LGI, respectively

Fig. 8 Undeformed
corresponding 2D
representation of the 3D
microstructure for SGI shown
to the *left* in Fig. 7

Conclusions

In the present paper, three-dimensional finite element models have been developed in order to better understand the effects of graphite inclusion morphology under similar loading conditions. The localization of plastic strain has been proven to be more pronounced for SGI than for the other two microstructures, CGI, and LGI. It has also been concluded that numerical analysis in two dimensions are not sufficient when analyzing actual microstructural features, which is common observed in literature. The effects originating from the three-dimensional representation of the microstructure is most likely the cause of mismatch between e.g. micro digital image correlation (μDIC) and finite element simulations trying to predict strain fields locally [11].

References

1. J.R. Davis, *Cast irons*, (ASM International, Materials Park, Ohio, 1996)
2. J. Olofsson, I.L. Svensson, Incorporating predicted local mechanical behaviour of cast components into finite element simulations. Mater. Design. 34, 494–500 (2012)
3. J. Olofsson, I.L. Svensson, The effects of local variations in mechanical behaviour—numerical investigation of a ductile iron component. Mater. Design, 43, 264–271 (2013)

4. U. Riebel, V. Kofler, F. Löffler, Shape characterization of crystal and crystal agglomerates. Part. Part. Syst. Charact. 8, 48–54 (1991)
5. Y. Tanaka, H. Saito, I. Tokura, K. Ikawa, Relationship between some physico-mechanical properties and numerical indexes of graphite shape in compacted-vermicular graphite cast irons. Trans. ASME **104**, 60–65 (1982)
6. H. Ledbetter, S. Datta, Cast iron elastic constants: effect of graphite aspect ratio. Z. Metallkd. **83**(3), 195–198 (1992)
7. S.H. Pundale, R.J. Rogers, G.R. Nadkarni, Finite element modelling of elastic modulus in ductile irons: effect of graphite morphology. AFS Trans. **98–102**, 99–105 (2000)
8. K.M. Pedersen, N.S. Tiedje, Graphite nodule count and size distribution in thin-walled ductile cast iron. Mater. Charact. **59**, 1111–1221 (2008)
9. T. Owadano, Graphite nodule number in spheroidal graphite and malleable cast irons. Imono/Jpn Foundrymen's Soc **45**, 193–197 (1973)
10. C. Fragassa, N. Radovic, A. Pavlovic, G. Minak, Comparison of mechanical properties in compacted and spheroidal graphite irons. Tribol. Ind. **38**(1), 49–59 (2016)
11. K. Kasvayee, K. Salomonsson, E. Ghassemali, A. Jarfors, Microstructural strain distribution in ductile iron; comparison between finite element simulation and digital image correlation measurements. Mater. Sci. Eng. A **655**, 27–35 (2015)
12. G. Fischer, J. Nellesen, N.B. Anar, K. Ehrig, H. Riesemeier, W. Tillmann, 3D analysis of micro-deformation in VHCF-loaded nodular cast iron by & #x03BC;CT. Mater. Sci. Eng. A **577**, 202–209 (2013)
13. M. Abouridouane, F. Klocke, D. Lung, Microstructure-based 3D FE modeling for micro cutting ferritic-pearlitic carbon steels. In *Proceedings of ASME 2014 Manufacturing Science and Engineering Conference MSEC2014*, Detroit, Michigan, USA. MSEC2014-4011 9–13 June 2014
14. T. Sjögren, I.L. Svensson, Modelling the Effect of Graphite Morphology on the Modulus of Elasticity in Cast Irons. In *International Journal of Cast Metals Research*, **17**(5), 271–279 (2004)
15. V.I. Litovka, N.I. Bekh, O.I. Shinskii, N.I. Tarasevich, P. Yakovlev, G.A. Kosnikov, Effects of composition and structure on the state, fatigue and damping properties of high-strength cast iron. Strength Mater. **27**(8), 448–453 (1995)
16. Y.B. Zhang, T. Andriollo, S. Fœster, W. Liu, J. Hattel, R.I. Barabash, Three-dimensional local residual stress and orientation gradients near graphite nodules in ductile cast iron. Acta Mater. **121**, 173–180 (2016)